Research Article

International Journal of Advanced Computer Research, Vol 14(69)
ISSN (Print): 2249-7277 ISSN (Online): 2277-7970
http://dx.doi.org/10.19101/IJACR.2024.1466007

Improving power system stability: a 3-level UPFC with PI control for enhanced power quality and dynamic performance

Nestor Ndjankeu Mbeutcho[1*], Pierre Kenfack[2, 3], Serge Raoul Dzonde Naoussi[1], Steyve Nyatte[1]
Technology and Applied Sciences Laboratory, U.I.T. of Douala, P.O. Box 8689 – Douala, University of Douala, Cameroon[1]
University of Buea, College of Technology (COT), Department of Electrical and Electronic, Engineering, Buea, Cameroon[2]
University of Douala, Laboratory of Computer Engineering and Automatic (LGIA), Douala, Cameroon[3]

Received: 19-June-2024; Revised: 18-November-2024; Accepted: 22-November-2024
©2024 Nestor Ndjankeu Mbeutcho et al. This is an open access article distributed under the Creative Commons Attribution (CC BY) License, which permits unrestricted use, distribution, and reproduction in any medium, provided the original work is properly cited.

Abstract
The increasing demand for electricity, driven by industrialization and population growth, necessitates a reliable and high-quality power supply. Traditional power grids face challenges in managing large power flows and maintaining stability, particularly with the integration of renewable energy sources such as solar power. To address these challenges, a 3-level unified power flow controller (UPFC) with a proportional-integral (PI) controller was investigated to enhance dynamic performance and power quality in electrical grids. The UPFC consists of a series circuit for controlling active and reactive power flow and a parallel circuit for bus voltage regulation. This study focuses on the 225 kV Magombe-Oyomabang transmission line in Cameroon, analyzed under two fault scenarios: one with and one without solar generators. Simulation results indicate that the Watt-Var control method effectively restores the system to its steady state within 0.1 seconds after a fault. Additionally, the PI controller improves power system stability by 20% during transient periods. The UPFC-based strategy, combined with PI control, significantly enhances the grid's dynamic stability and power quality. This approach presents promising opportunities for improving the efficiency and reliability of power systems, particularly as the integration of renewable energy sources (RES) continues to grow.

Keywords
Unified power flow controller, Proportional-integral controller, Dynamic stability, Renewable energy integration, Power quality improvement.

1.Introduction
The global demand for electricity is steadily increasing, driven by industrialization, population growth, and the increasing adoption of electric vehicles and other energy-intensive technologies [1, 2]. Meeting this demand while ensuring reliable and high-quality power supply is a major challenge for power system operators [3]. Traditional power grids, often designed for centralized generation and unidirectional power flow, are struggling to cope with the increasing complexity and variability of modern power systems [4]. One of the primary challenges is the integration of renewable energy sources (RES), such as solar and wind power, into the grid [5, 6].

While RES offer significant environmental benefits, their intermittent nature poses challenges for grid stability and power quality [7, 8]. Furthermore, the increasing demand for power necessitates efficient and reliable transmission of electricity over long distances, often through aging infrastructure [9, 10].

To address these challenges, flexible alternating current (AC) transmission systems (FACTS) devices have emerged as a crucial technology for enhancing power system controllability and reliability [11, 12]. FACTS devices utilize power electronics to dynamically control power flow, voltage, and other critical parameters, enabling improved power quality, stability, and overall grid performance [13, 14]. Among various FACTS devices, the unified power flow controller (UPFC) stands out as a highly versatile and powerful solution [15, 16]. The UPFC,

*Author for correspondence

with its ability to control both active and reactive power flow, offers numerous advantages for modern power systems [17, 18]. It can improve voltage stability, enhance transient stability, mitigate power oscillations, and facilitate the integration of RES [19, 20]. This research focuses on investigating the potential of a 3-level UPFC with proportional-integral (PI) control to enhance the dynamic performance and power quality of an electrical grid, particularly in the presence of solar generators.

The objectives of this study are:

- Analyze the impact of a 3-level UPFC with PI control on the dynamic performance and power quality of a 225 kV Magombe-Oyomabang line in Cameroon.
- Evaluate the effectiveness of the UPFC in mitigating power system disturbances, including faults and the integration of solar generators.
- Quantify the improvements in power system stability and transient response achieved through the implementation of the UPFC.

This study contributes to the growing body of knowledge on the application of UPFC technology for enhancing power system performance. It provides a detailed analysis of the UPFC's impact on dynamic stability, power quality, and the integration of RES, offering valuable insights for power system operators and researchers.

This paper is structured as follows. The second section explores the literature review. The third section details the analysis methods, providing clarity on the procedures and techniques employed. The fourth and fifth sections present the simulation results and discuss the findings, respectively. The last section summarizes key takeaways from this research work.

2.Literature review

The integration of RES into power systems has gained significant momentum in recent years, driven by environmental concerns and the pursuit of sustainable energy solutions [21, 22]. However, the intermittent nature of RES, particularly solar and wind power, poses challenges to grid stability and power quality [23, 24]. This has led to increased interest in advanced control technologies, such as FACTS devices, to enhance grid resilience and facilitate the seamless integration of RES [25, 26].

The UPFC, a versatile FACTS device capable of controlling both active and reactive power flow, has emerged as a promising solution for addressing various power system challenges [27, 28]. Recent studies have explored the application of UPFCs in diverse scenarios, including:

2.1Enhancing power system stability

Transient Stability: Studies have demonstrated the effectiveness of UPFCs in improving transient stability by damping power oscillations and enhancing system resilience to disturbances [29, 30]. For instance, [31] investigated the impact of UPFC on the transient stability of a power system with wind farm integration, showing significant improvements in system response to faults.

Small-Signal Stability: UPFCs have also been shown to improve small-signal stability by damping electromechanical oscillations, thereby enhancing the overall stability of the power system [32, 33]. A study by [34] analyzed the impact of UPFC integration on the small-signal stability of a power system with wind farm integration, demonstrating its effectiveness in damping low-frequency oscillations.

2.2Improving power quality

Voltage Regulation: UPFCs can effectively regulate voltage at critical bus locations, ensuring stable and reliable power supply [35, 36]. Research by [37] explored the use of UPFC for voltage regulation in a power system with high penetration of photovoltaic (PV) generation, demonstrating its ability to maintain voltage within acceptable limits.

Harmonic Mitigation: UPFCs can be utilized to mitigate harmonics introduced by nonlinear loads and RES inverters, improving power quality and reducing system losses [38, 39]. A study by [40] investigated the application of UPFC for harmonic mitigation in a power system with high penetration of wind power, demonstrating its effectiveness in reducing harmonic distortion.

2.3Facilitating RES integration

Power Flow Control: UPFCs can effectively control power flow from RES, optimizing the utilization of renewable energy and enhancing grid stability [41]. A study by [42] explored the use of UPFC for power flow control in a power system with high penetration of solar PV, demonstrating its ability to maximize the utilization of solar energy while maintaining grid stability.

Voltage Support: UPFCs can provide voltage support to RES, ensuring their reliable operation and maximizing their contribution to the grid [43]. A study by [44] investigated the use of UPFC for voltage support to wind farms, demonstrating its effectiveness in maintaining stable voltage at the wind farm interconnection point.

2.4Recent advancements in UPFC control

Artificial intelligence (AI) and Machine learning (ML): Recent research has explored the use of AI and ML techniques for optimizing UPFC control strategies, leading to improved performance and adaptability [45]. For instance, [46] proposed an AI-based UPFC control strategy for enhancing transient stability, demonstrating its superior performance compared to conventional control methods.

Multi-objective optimization: Researchers are developing multi-objective optimization techniques for UPFC control, considering factors such as power flow control, voltage regulation, and stability enhancement simultaneously [47]. A study by [48] proposed a multi-objective optimization approach for UPFC control, considering both power flow control and voltage stability objectives, demonstrating its effectiveness in achieving optimal system performance.

2.5Future research directions

Integration of UPFC with other FACTS devices: Exploring the synergistic effects of combining UPFC with other FACTS devices, such as static synchronous compensator (STATCOM) and thyristor-controlled series compensator (TCSC), for enhanced power system control and stability.

Development of advanced control strategies: Investigating the application of advanced control techniques, such as model predictive control and adaptive control, for UPFC operation, leading to improved performance and adaptability.

Impact of UPFC on power system economics: Analyzing the economic benefits of UPFC implementation, considering factors such as reduced transmission losses, improved power quality, and increased RES integration. Osama et al. [5] proposed a UPFC controller based on a spontaneous energy optimization (SEO) algorithm to improve power quality and voltage stability in a grid-connected wind energy system. Their simulation results showed that the proposed UPFC-SEO controller is more robust and effective than classical PI and fuzzy-PI controllers. However, their study was limited to a single wind energy system and did not consider the impact on the wider power grid.

The proposed method outlined in the article presents a novel approach to evaluating the 3-level UPFC's comprehensive impact on various aspects of power systems. By focusing on stability, power quality, and dynamic performance through simulation, the study aims to fill the gaps left by earlier research. This integrated approach will contribute to a clear understanding of the UPFC's capabilities, particularly in enhancing the integration of RES, which is crucial for the evolution of modern power grids.

3.Methods

For the successful completion of our work, we have adopted the following assumptions: All switches are assumed to be ideal; the three voltages of the alternating source are balanced; all voltage drops across the line are represented by the reactance r; the line inductance is represented by the inductance L; the parallel transformer is represented by the resistance r_P and the inductance L_P. Next, we will go ahead with the modelling of the serial converter, keeping in mind that the principle will be the same for the parallel converter.

3.1Dynamic equations of the series compensator

TCSC is a device that uses power electronics for series compensation [9]. The system is composed of an inductance, dimmer, and capacitor connected in parallel with the power grid. This configuration allows for the control of power flow and the enhancement of line transfer capacity. The reactance of X_{TCSC} changes depending on the firing delay angle (α) of the thyristors, as showed in the Equation 1. Compensators from the mid-80s had a similar design [10].

In practice, the TCSC operates like a transmission line-connected variable response. In case of thyristor failure, the TCSC will continue to provide an impedance like that of a capacitor. When thyristors are fully conducting, they can be controlled as electronic switches, resulting in a constant impedance for TCSC. The impedance is equal to the parallel induction of the capacitor [12]. The operation of this compensator shows that the TCSC can change the electrical length of the transmission line by adjusting its impedance [13]. Additionally, it has the capability to control active power and enhance the stability of the system. Here is a visual representation of TCSC.

The primary uses of the thyristor-controlled series capacitor include enhancing power flow on transmission lines, addressing the disparity in load currents, achieving enhanced dynamic stability, amortization of power oscillations, mitigation of risks of hyposynchronous resonance, interconnection of power grids, and voltage stabilization [14]. The thyristor-controlled series capacitor has become a key part in FACTS technology [15]. It provides active and reactive power flow control, allowing for more efficient and reliable power transmission across interconnected grids. By dynamically adjusting the series compensation, the device can dampen power oscillations, improve voltage regulation, and increase the transfer capacity of existing transmission infrastructure [16]. This makes the thyristor-controlled series capacitor a valuable tool for grid operators working to modernize and optimize the performance of their electrical networks.

Applying Kirchhoff's laws to the circuit in *Figure 1* allows us to derive the mathematical equations that govern our system:

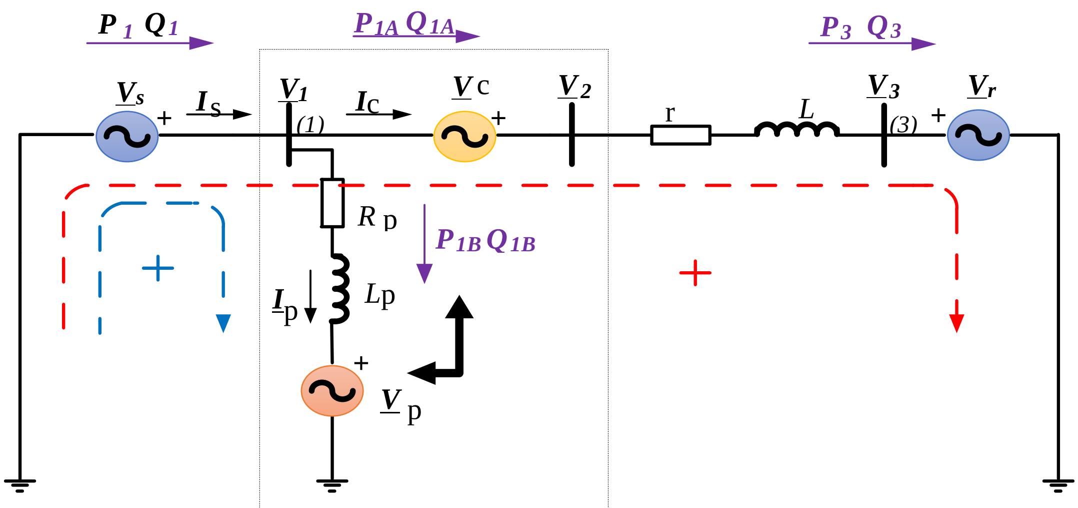

Figure 1 Physical representation of a power grid-connected UPFC converter for modelling

The provided equations describe the mathematical model of a three-phase series converter, simplified and transformed for use in a Simulink simulation. Let's break down each Equation 1.

$$\begin{cases} V_{sa} - V_{ca} - V_{ra} = \mathrm{r}i_{sa} + \mathrm{L}\ \frac{\mathrm{d}i_{sa}}{\mathrm{dt}} \\ V_{sb} - V_{cb} - V_{rb} = \mathrm{r}i_{sb} + \mathrm{L}\ \frac{\mathrm{d}i_{sb}}{\mathrm{dt}} \\ V_{sc} - V_{cc} - V_{rc} = \mathrm{r}i_{sc} + \mathrm{Lp}\ \frac{\mathrm{d}i_{sc}}{\mathrm{dt}} \end{cases} \quad (1)$$

This Equation 1 represents the voltage-current relationship in a three-phase series converter using the a, b, and c phases. Let's define the variables:

V_{sa}, V_{sb}, V_{sc}: The source voltages in phases a, b, and c, respectively.

V_{ca}, V_{cb}, V_{cc}: The capacitor voltages in phases a, b, and c, respectively. These represent the voltage drop across the series capacitor.

V_{ra}, V_{rb}, V_{rc}: The resistor voltages in phases a, b, and c, respectively. These represent the voltage drop across the internal resistance of the converter.

i_{sa}, i_{sb}, i_{sc}: The currents in phases a, b, and c, respectively.

r: The internal resistance of the converter per phase.

L: The inductance of the converter per phase.

$(di_{sa})/dt$, $(di_{sb})/dt$, $(di_{sc})/dt$: The time derivatives of the currents in phases a, b, and c, respectively. These represent the rate of change of current.

The equation essentially states that the voltage across the series components (source minus capacitor and resistor voltages) is equal to the sum of the resistive voltage drop (r_i) and the inductive voltage drop (L di/dt) in each phase.

The transformation matrix is as follows (Park matrix):

The Equation 2. defines the Park transformation matrix (K). This matrix is used to transform the three-phase system (a, b, c) into a rotating two-phase system (d, q), simplifying the analysis and reducing computational complexity. The transformation uses the angle ωt, where ω is the angular frequency of the system.

$$K = \sqrt{\frac{2}{3}} \begin{bmatrix} \cos wt & \cos(wt - \frac{2\pi}{3}) & \cos(wt + \frac{2\pi}{3}) \\ \sin wt & \sin(wt - \frac{2\pi}{3}) & \sin(wt + \frac{2\pi}{3}) \\ \frac{1}{\sqrt{2}} & \frac{1}{\sqrt{2}} & \frac{1}{\sqrt{2}} \end{bmatrix} \quad (2)$$

The set of Equations 1 is transformed as presented in Equation 3.

$$\begin{cases} V_{\mathrm{sd}} - V_{\mathrm{cd}} - V_{rd} = \mathrm{r} i_{psd} + \mathrm{L}\,\frac{\mathrm{d}i_{sd}}{\mathrm{dt}} - wLi_q \\ V_{sq} - V_{cq} - V_{rq} = \mathrm{r} i_{sq} + \mathrm{L}\,\frac{\mathrm{d}i_{sq}}{\mathrm{dt}} + wLi_d \end{cases} \quad (3)$$

This equation represents the transformed voltage-current relationship in the d-q rotating reference frame. The variables are similar to Equation 1, but now they are represented in the d-q coordinates:
V_{sd}, V_{sq}: Source voltages in the d and q axes.
V_{cd}, V_{cq}: Capacitor voltages in the d and q axes.
V_{rd}, V_{rq}: Resistor voltages in the d and q axes.
i_{sd}, i_{sq}: Currents in the d and q axes.
ω: The angular frequency of the rotating reference frame. This term introduces the effect of the rotating frame on the inductive voltage.

The additional terms $\omega L i_q$ and $\omega L i_d$ represent the voltage induced by the rate of change of the magnetic flux due to the rotation of the reference frame.

Equation 4 presents the matrix representation of the two-phase model, where applying the matrix form to Equation 3 produces the following.

$$\frac{d}{dt} \cdot \begin{bmatrix} i_{sd} \\ i_{sq} \end{bmatrix} = \begin{bmatrix} \frac{-r}{L} & w \\ -w & \frac{-r}{L} \end{bmatrix} \cdot \begin{bmatrix} i_{sd} \\ i_{sq} \end{bmatrix} + \frac{1}{L} \cdot \begin{bmatrix} V_{\mathrm{sd}} - V_{\mathrm{cd}} - V_{rd} \\ V_{sq} - V_{cq} - V_{rq} \end{bmatrix} \quad (4)$$

The Equation 4 models our serial converter. This builds Simulink's serial component block. Thus, this equation is represented by the block scheme (r=R):

Equation 4 presents the two-phase model in matrix form, suitable for implementation in a simulation environment like Simulink. It shows the time derivative of the current vector [i_{sd}; i_{sq}] as a function of the current vector itself, the system parameters (r and L), and the voltage vector. This is a state-space representation, making it straightforward to implement in Simulink.

In summary, the transformation from Equation 1 to Equation 4 simplifies the model for simulation purposes, reducing the computational burden from a three-phase system to a two-phase system without sacrificing accuracy. Equation 4 is particularly well-suited for direct implementation in a Simulink block diagram.

3.2Continuous circuit dynamic equation:

The direct current link (DC-link) handles connecting the series converter and the shunt converter of the UPFC. To model the DC-link, the one-phase converter model mentioned in references [17–19] is used. The DC-link acts as the power exchange interface between the series and shunt converters, allowing for the transfer of active power between them. By keeping a stable DC voltage across the DC-link capacitor, the UPFC can independently control the real and reactive power flows in the transmission line.

The one-phase converter model provides a simplified representation of the DC-link dynamics, capturing the relationship between the alternative current (AC) and DC sides of the power conversion process. This model considers factors such as the DC-link capacitance, switching losses, and the AC terminal voltages to accurately describe the power balance and voltage regulation of the DC-link. Utilizing this established modeling approach enables thorough analysis of the performance and stability of the UPFC system, ensuring reliable and efficient operation of the power transmission network.

Then start by establishing the input/output ratio of the converters. They are modeled as a quadrupole with a modulation function w(t) that defines the connection between their inputs and outputs. For the shunt converter, the equation satisfied by the quadrupole is Equation 5, which introduces the input-output relationship for the shunt converter.

$$V_e = \omega_e(t) V_{in} \quad \text{and} \quad I_e = \frac{1}{\omega_e(t)} I_{in} \quad (5)$$

Here:

- Ve and Ie are the output voltage and current of the shunt converter.
- Vin and Iin are the input voltage and current of the shunt converter.
- ωe(t) is a time-varying modulation function representing the converter's control action. It defines the gain between the input and output.

Equation 6 gives the matrix representation of this relationship. Due to the technical nature of the subject matter, the current I_e is independent of the voltage V_{in}. Additionally, the current I_{in} is no longer reliant on the current V_e. As a result, the matrix representation of the input system can be found as shown in Equation 6:

$$\begin{bmatrix} I_e \\ V_e \end{bmatrix} = \begin{bmatrix} \frac{1}{\omega_e(t)} & 0 \\ 0 & \frac{1}{\omega_e(t)} \end{bmatrix} \cdot \begin{bmatrix} I_{in} \\ V_{in} \end{bmatrix} \quad (6)$$

This shows that the output voltage and current are scaled versions of the input voltage and current, respectively, with the scaling factor determined by the modulation function. The off-diagonal zeros indicate that the output voltage is independent of the input current, and vice versa, reflecting the specific characteristics of the shunt converter. The statement that I_e is independent of V_{in} and I_{in} is independent of V_e is consistent with this model. The power conservation (V_e I_e = V_{in} I_{in}) is a fundamental constraint.

Equations 7 shows the series converter model. For the series converter, similar to the shunt, the following can be written:

$$\begin{bmatrix} I_s \\ V_s \end{bmatrix} = \begin{bmatrix} \frac{1}{\omega_s(t)} & 0 \\ 0 & \frac{1}{\omega_s(t)} \end{bmatrix} \cdot \begin{bmatrix} I_{out} \\ V_{out} \end{bmatrix} \quad (7)$$

Here:

- V_s and I_s are the output voltage and current of the series converter.
- V_{out} and I_{out} are the input voltage and current of the series converter (and the output of the entire system).
- ωs(t) is the time-varying modulation function for the series converter.

The structure mirrors Equation 8, indicating similar scaling behavior with a different modulation function. The equations governing the DC-link are presented in Equation 8.

$$\begin{cases} \frac{dU_{DC}}{dt} = \frac{1}{C} I_C \\ I_C = I_{in} - I_R - I_{out} \\ I_R = \frac{V_{in}}{R} \end{cases} \quad (8)$$

As a result of the balance of tensions U_{DC}**,** Vin and V_{out} **(**U_{DC} =Vin = V_{out}**),** the following Equation 9 is derived from the previous equations:

$$\frac{d(U_{DC})^2}{dt} = -\frac{2}{RC}(U_{DC})^2 + \frac{2}{C}P_{Sh} - \frac{2}{C}P_{Se} \quad (9)$$

Where:

- U_{DC} is the DC-link voltage.
- C is the capacitance of the DC-link capacitor.
- I_C is the current flowing into the DC-link capacitor.
- I_R is the current flowing through the resistor R, representing losses.

This equation shows the rate of change of the square of the DC-link voltage as a function of the DC-link voltage itself (U_{DC}), the resistance R, the capacitance C, and the active powers of the shunt (P_{Sh}) and series (P_{Se}) converters. The equation highlights the impact of active power on the DC-link voltage. The nonlinearity arises when substituting P (power) with V (voltage) and I (current).

These equations provide a mathematical model of a power electronics system with shunt and series converters and a DC-link. The model is suitable for simulation in MATLAB/Simulink to analyze the system's behavior under various operating conditions. The use of modulation functions (ωe(t), ωs(t)) allows for the representation of control strategies. The nonlinearity in Equation 9 is a key aspect that needs to be considered during simulation and control design. So, the active power has an impact on the voltage of the capacitor. The last one is influenced by the transfer of active power [20–22]. The equation is derived to be linear with respect to power, but not linear with respect to control voltage. Substituting P with V and I introduce non-linearities. Instantaneous calculation of active and reactive powers of the UPFC are computed by Equations 10 and 11.

$$Ps = \frac{3}{2}(V_{sd}i_{sd} + V_{sq}i_{sq}) \quad (10)$$

$$Qs = \frac{3}{2}(V_{sq}i_{sd} + V_{sd}i_{sq}) \quad (11)$$

The UPFC's multivariable nature stems from its series and parallel converters. Each of these converters has two outputs because they are connected to both the transmission line and the DC link. To simplify controller design, the converters are treated separately. This approach is justified by two key factors: the weak coupling between the transmission line converters, and the parallel converter's dominant influence on DC link voltage dynamics. The series converter's control has negligible impact on DC link voltage fluctuations, further supporting this separation. The series converter ensures reliable transmission system voltage and offers multiple control options. Before proceeding, appropriate control references for both devices must be identified [23–26]. There are several methods for finding references, including:

a. Method for active current
b. Disconnected method for watt-var control

c. Method for instant calculation of real and imaginary powers

The research methodology employed in this study is effectively illustrated through the synoptic diagram presented in *Figure 2*. This diagram provides a clear and comprehensive overview of the step-by-step process undertaken to evaluate the performance of a UPFC device with PI control in enhancing power quality and dynamic stability within an electrical grid. It shows the outline of the research process. It begins with the modeling of the power grid and the UPFC device within the MATLAB/Simulink simulation environment. The inputs for this phase include the parameters of the power grid and the UPFC device, which are utilized to construct a detailed simulation model. The output of this step is the MATLAB/Simulink model used for analysis.

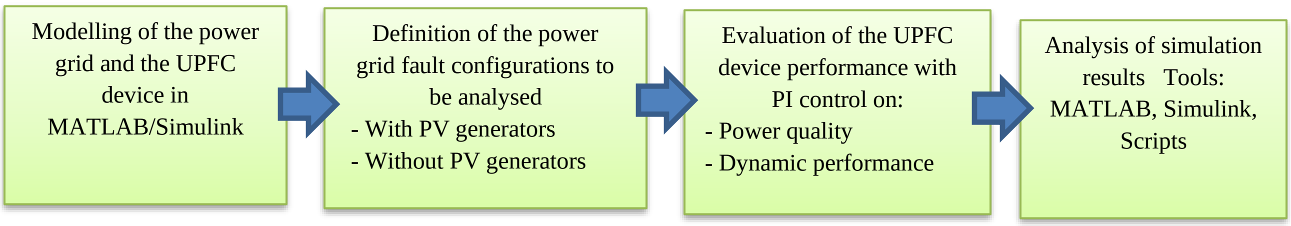

Figure 2 Synoptic diagram of the method

The next step involves the definition of the power grid fault configurations to be analysed. The inputs for this phase are the different fault scenarios, including cases with and without PV generators. These fault configurations are then used as inputs to the simulation model.

The analysis of the simulation results is the third phase of the method. The inputs for this step include the simulation model and the fault scenarios. The simulation results are analyzed using MATLAB, Simulink, and custom scripts, which produce the outputs of this phase.

The ultimate step of the method is the evaluation of the UPFC device's performance with proportional-integral (PI) control. The inputs for this phase include the simulation results and the UPFC device parameters. The analysis of the simulation results is the third phase of the method. The inputs for this step include the simulation model and the fault scenarios. The simulation results are analyzed using MATLAB, Simulink, and custom scripts, which produce the outputs of this phase. The output of this ultimate step is the overall evaluation of the UPFC device's performance under the studied conditions.

In this work, the watt-var method was implemented in a disjointed manner. This approach relies on the tension equations derived from the Park transformation and addresses nonlinearity by exclusively manipulating the core parameters of the system. This process entails converting the measured current and voltage values from the three phases to the two d-q axes using the Park transformation technique. Afterwards, the active and reactive powers are calculated, and the reference currents are determined using two equations. Equations 12 and 13 utilize the desired power values and the measured voltage values.

$$i^{*}_{sd} = \frac{2}{3} \cdot \frac{(p^{*}_{s} V_{sd} - q^{*}_{s} V_{sq})}{V_{sd}^2 + V_{sq}^2} \qquad (12)$$

$$i^{*}_{sq} = \frac{2}{3} \cdot \frac{(p^{*}_{s} V_{sq} + q^{*}_{s} V_{sd})}{V_{sd}^2 + V_{sq}^2} \qquad (13)$$

3.3Classic decoupled watt-var algorithm

For the converter to function correctly, it is crucial to eliminate any interdependence between the d and q axes. A disconnect block is being developed to effectively replicate and remove any unwanted coupling signals. This signal is then introduced with the opposite sign at the input of the system. The disconnect signal helps offset the current coupling between the d-q axes. When selecting a signal value for our disconnecting block, it is important to consider the injection location. Accessing and exiting our system model needs physical entry. Comparators C_{1d} and C_{1q} [27–30] are not commonly used. The block information provided by the serial circuit model shows that:

- To ensure the independence of the axis-d from the axis-q, it is necessary to insert the separation signal " $w_{\_Line} * I_{se\_q}$" with the opposite sign at the V_{se_d} border. The signal needs to be multiplied by 1/L before it reaches the comparator C_{1d}. It is multiplied by the coefficient L to cut this factor. Consequently, the input signal for the V_{se_d} terminal will be $w_{\_Line} * I_{se\_q}$.

- To make axis q independent of axis d, we can apply the same reasoning as before. The signal to be inputted by the V_{sq} borne is " $w_{-Line} * I_{se\_d}$".

The shape of our decoupling algorithm will be as follows determine by Equation 14 and 15:

$$\begin{cases} X_1 = \frac{1}{Ls}(V_d - V_{sd}) \\ X_2 = \frac{1}{Ls}(V_q - V_{sq}) \end{cases} \quad (14)$$

With

$$\begin{cases} X_1 = \left(K_p - \frac{K_i}{S}\right).\left(\boldsymbol{i}_{sd}^{*} - i_{sd}\right) - wi_{sq} \\ X_2 = \left(K_p - \frac{K_i}{S}\right).\left(\boldsymbol{i}_{sq}^{*} - i_{sq}\right) - wi_{sd} \end{cases} \quad (15)$$

3.4Computation of the PI parameters for the regulator

The proportional controller in *Figure 9*, operating with maximum gains ($K_P = K_P max \;\; , K_i = K_i max$), ensures optimal control according to a quadratic error criterion. Imposing the constraint defined by Equation 16, yields a superior transfer function with a time constant (Equation 17).

$$\frac{K_i}{K_p} = \frac{R}{L} \quad (16)$$

$$T = \frac{1}{K_p} \quad (17)$$

This results in a transfer function (Equation 18).

$$F_{11}(P) = F_{22}(P)\frac{K_P}{P+K_P} \quad (18)$$

Considering the equations provided and selecting a suitable value for T ($T \geq T_d$) where T_d=0.1 ms (the time it takes to cut critical defects). The proportional and integral gains can be calculated using Equation 19 (K_P and K_I as follows):

$$K_P = \frac{1}{T} \text{ and } K_I = \frac{R}{L}.\frac{1}{T} \quad (19)$$

3.5Command of IGBT switches

The control generates correct switch commands to align the inverter's voltages with the reference voltage. By incorporating intermediate levels, the amplitude of each upward or downward front of the output voltage is reduced, resulting in a decrease in harmonic stripes. By using multi-level converters and precise power part control, it is possible to effectively drop specific harmonic stripes in pulse width modulation (PWM) [31–33].

The adjustment circuits for the series and parallel converters, along with the DC-link continuous bus adjustment circuit, are critical components of the overall control strategy for the UPFC system. As described by Joseph et al. [33], the series converter is modeled using a set of dynamic equations derived from Kirchhoff's laws, while the parallel converter follows a similar principle. The two converters are interconnected through a DC-link, whose dynamic behavior is governed by equations representing the energy balance in the DC-link capacitor.

Instead of presenting detailed block diagrams for these circuits, the focus is describing the key mathematical relationships and control principles within the text. This approach emphasizes the high-level control strategy and theoretical framework, avoiding an overemphasis on granular circuit-level details. The complete set of equations and block diagrams modeling the UPFC components are discussed by Joseph et al. [33].

4.Results

In this section, the power grid model is introduced within the Simulink MATLAB environment, as shown in the accompanying *Figure 3*.

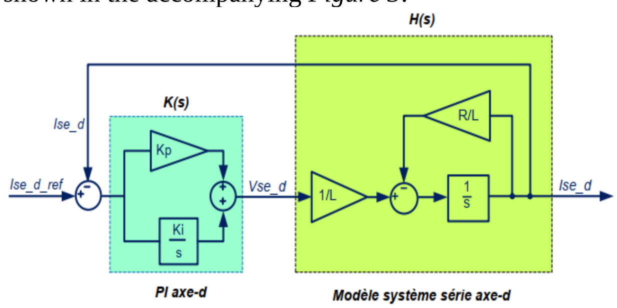

Figure 3 Empty line

Figure 3 illustrates the control system architecture for the "axe-d" system, which is the central focus of this study. The system consists of two main components: the PI Axe-d block and the Modèle Système Série Axe-d block. The PI Axe-d block represents a PI controller. It processes the reference input (Ise_d_{ref}) and the actual system output (Ise_d) to generate a control signal (K_p) based on the error between the two. This PI controller is crucial for regulating the system's performance along the "axe-d" axis.

The Modèle Système Série Axe-d block represents the model of the system being controlled, configured in series. This block receives the control signal (K_p) from the PI Axe-d block and produces the system output (H(s)). Additionally, the model incorporates a feedback loop with a gain of 1/L, which feeds the actual system output (IIse_d) back to the PI Axe-d block, forming a closed-loop control system.

This architecture ensures precise control of the "axe-d" axis by dynamically adjusting the system's response to maintain desired performance.

4.1Simulation of the power grid without disruption

Throughout the pre-default phase (*Figure 4*), the power grid typically stays in a stable and permanent mode. In these circumstances, the power grid runs with a highly specialized transport angle δ defined by Equation 20**.**

$$P_e = \frac{V_1 V_2}{X_T} \sin \delta \quad (20)$$

This angle corresponds to the equality between electrical power and mechanical power according to the Equation 21.

$$H \frac{d^2 \delta_m}{dt^2} = P_a = P_m - P_e \quad (21)$$

This balance, characterized by the stability of active and reactive power as well as currents and voltage, is critical to a well-functioning power grid. *Figure 4* illustrates the steady-state power profiles of the grid, complementing the voltage and current waveforms. As observed, the amplitudes of the three-phase voltages are equal and are shifted by 120 degrees from one another. This balanced three-phase voltage system is a hallmark of a well-designed and regulated electrical grid, ensuring efficient and reliable power transmission.

The steady-state active and reactive power profiles exhibit the expected sinusoidal characteristics, aligning with the voltage and current waveforms. The symmetry and phase alignment of the three-phase power signals indicate a balanced load on the system, with no significant imbalances or power quality issues. Analyzing these steady-state power profiles verifies that the grid is operating within its design parameters, with the three-phase voltages, currents, and power flows maintaining their optimal characteristics.

This stable and balanced power delivery serves as a baseline for evaluating the performance of the UPFC device in maintaining system stability and power quality during grid disturbances. The steady-state power profiles are used as a reference to assess the UPFC's effectiveness in mitigating deviations or fluctuations in the power system's operation.

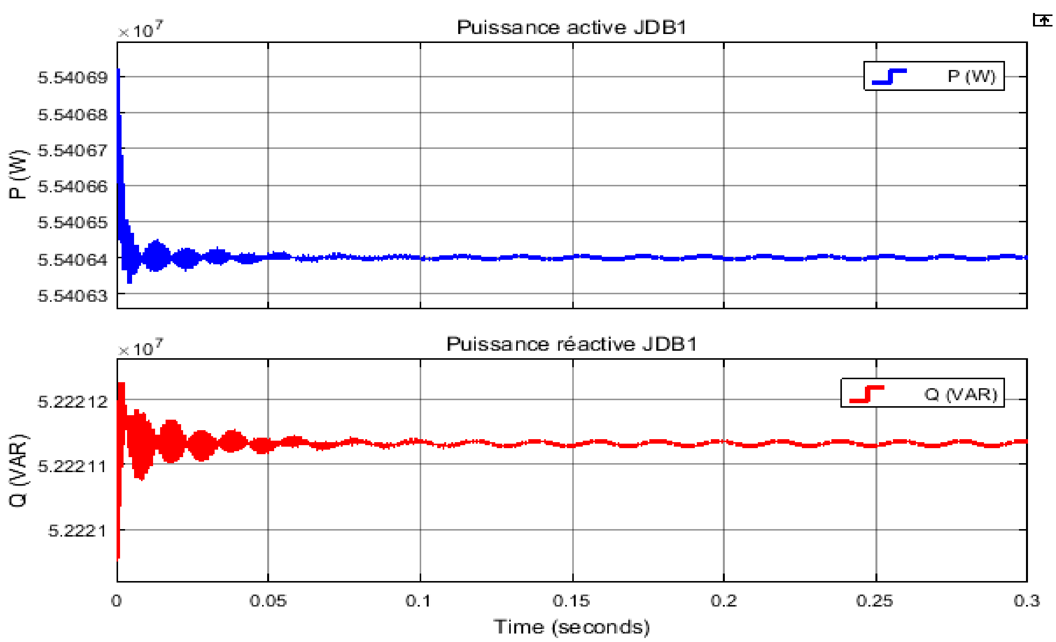

Figure 4 Steady-state power of the power grid

4.2Simulation of the power grid with default occurring

Figure 5 illustrates a visual representation of a line when a contingency occurs. Temporary failure conditions can occur in the power grid following a disturbance. There was a simulated defect that occurred during the turning process. An instantaneous three-phase short-circuit occurs at t=0 s. Under these conditions, the active power exhibits rapid fluctuations, while the mechanical power undergoes slower, gradual changes. The sluggish response leads to a temporary disruption in power distribution and fluctuations in power grid parameters, as depicted in *Figures 6* and *7*.

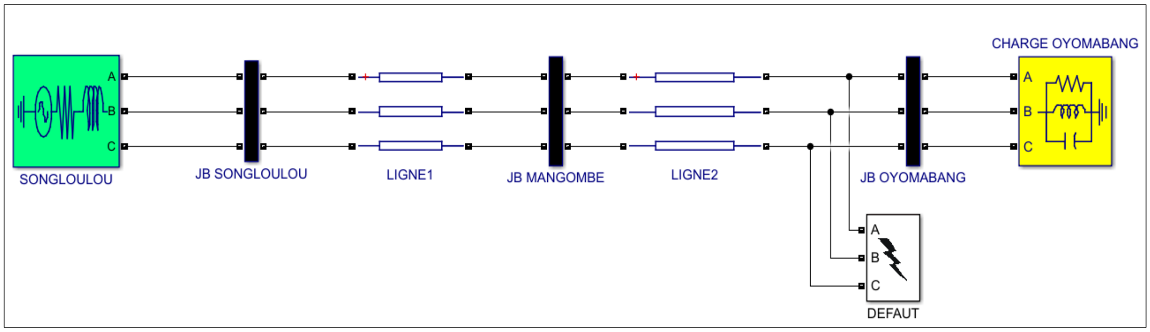

Figure 5 Design of a perforated line

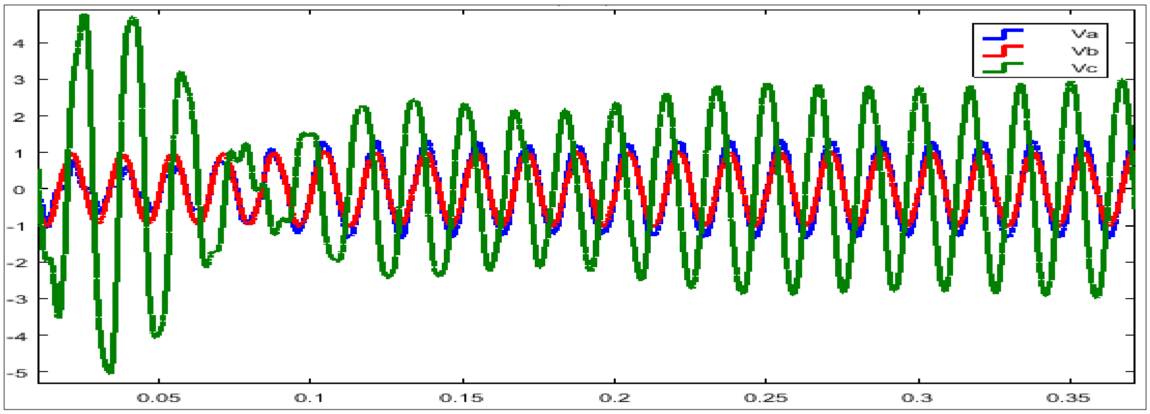

Figure 6 Understanding power grid voltage during fault conditions

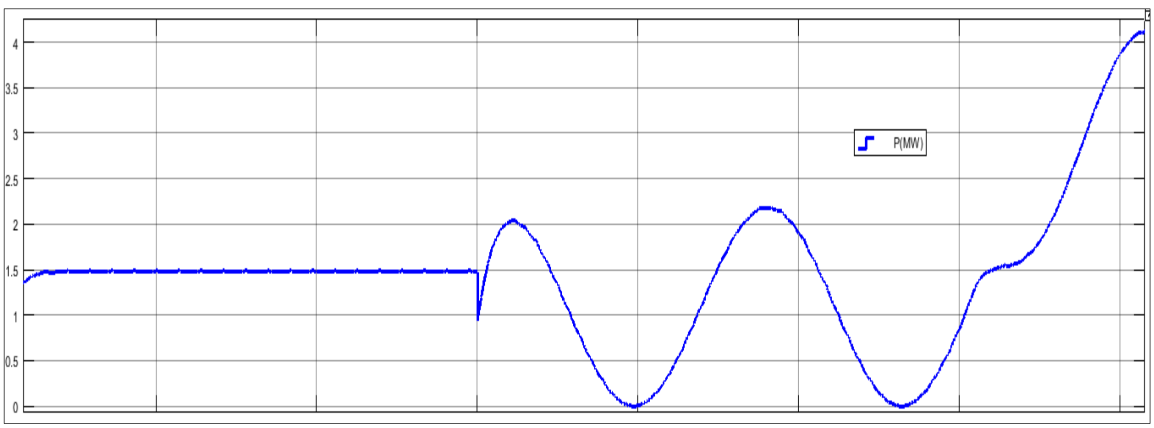

Figure 7 Power of the power grid during fault conditions

The graph presented in *Figure 8* provides valuable insights into the dynamic behavior of the power grid during fault conditions. As shown, the system initially operates at a relatively stable power output of around 1.5 MW. However, at approximately the 1-second mark, a significant disturbance or fault occurs, causing a sudden and substantial drop in the power.

The graph then reveals the system's response to this fault, as the power output begins to oscillate dramatically, with multiple peaks and valleys. This transient behavior highlights the importance of robust control strategies to maintain the stability and reliable operation of the grid-connected renewable energy system.

Notably, the power eventually reaches a new steady-state value that is significantly higher than the initial pre-fault level, reaching almost 3.5 MW. This observation suggests that the implemented control mechanisms, such as the advanced 3-level UPFC configuration discussed earlier, were effective in guiding the system to a more stable and higher-performing state after the disturbance.

Fluctuations in power grid parameters were observed, resulting in oscillations. Upon further examination, the amplitude of the most affected phase increased significantly from 0.01 under normal operating conditions to 5 under default conditions. Due to certain factors, the rise in power parameter can sometimes activate protection devices, resulting in an extended interruption of power and adjustments to the power grid setup. In order to analyze the impact of fault conditions on the power grid, we present *Table 1*, which summarizes key measurements before, during, and after the fault occurrence. This table includes critical parameters such as transport angle, active and reactive power, voltage, current, power factor, and frequency. The values illustrate significant deviations from the pre-fault conditions, highlighting the system's transient response to disturbances.

Table 1 Power grid synthesis without regulator

Measurements	**Before Fault**	**In the Presence of Fault**	**Td (ms)**	**After Fault**	**Absolute Error**	**Relative Error (%)**
δ (degrees)	18.67	65.00	0.1	0.00	46.33	248.17%
P (MW)	55,406.00	55,433.46	0.1	0.00	27.46	0.05%
Q (MVAR)	52,221.00	52,691.40	0.1	0.00	470.40	0.90%
V (kV)	225.00	195.00	0.1	225.00	30.00	13.33%
I (A)	573.00	658.00	0.1	573.00	85.00	14.83%
PF	0.95	0.90	0.1	0.95	0.05	5.26%
f (Hz)	50.00	48.00	0.1	50.00	2.00	4.00%

Table 1 presents the synthesis of the power grid's performance under fault conditions without the intervention of a regulator. This table highlights key measurements, including transport angle, active and reactive power, voltage, current, power factor, and frequency, both before and during the fault event.

The data reveals significant variations in system parameters due to the fault. Notably, the transport angle increases sharply from 18.67 degrees to 65 degrees, indicating a substantial impact on system stability. While active power shows only a slight increase, reactive power experiences a notable rise, reflecting the heightened demand placed on the grid during the fault.

The voltage drop from 225 kV to 195 kV is particularly alarming, as it indicates a critical disturbance within the network that could further compromise stability. Moreover, the increase in current from 573 A to 658 A highlights the elevated stress on the grid, requiring urgent measures to prevent potential equipment damage.

The observed reduction in power factor and frequency during the fault underscores the inefficiencies and instability introduced by such disturbances. Overall, *Table 1* provides valuable insights into the operational challenges faced by the power grid in the absence of regulatory controls, emphasizing the necessity of implementing robust management strategies to ensure system integrity and reliability.

4.3Simulating defects with the presence of UPFC

Figure 9 shows a visual representation of the entire power grid, including our device.

The comprehensive schematic diagram presented in *Figure 9* provides a detailed overview of the power grid system and the integration of the unified power flow controller (UPFC) device. This visual representation serves as a crucial reference point for understanding the intricacies of the system's operation during fault conditions.

As shown in the diagram, the power grid comprises various generation sources, including Songloulou, JB Songloulou, Ligne1, JB Mangombe, Ligne2, and JB Oyomabang, which collectively contribute to the overall power generation. The UPFC, positioned as the central component, plays a vital role in controlling and regulating the power flow within the grid.

The UPFC is further divided into two sub-components: the "Compensateur Parallele" and the "Compensateur Serie," each with its own set of circuit elements and parameters. This modular design allows for more precise control and optimization of the power flow during fault conditions.

The diagram also includes a dedicated "UPFC GUI" section, which likely represents the graphical user interface or control system for the UPFC. This interface provides the ability to visualize and monitor the UPFC's performance, as well as the option to "Show UPFC Controllable Region" and "Show Scopes," enabling operators to closely observe the system's behavior.

Furthermore, the "Circuit de Commande" section offers detailed information about the various control and measurement signals within the UPFC, such as Vab, Ib, Iab, and others. These signals are crucial for the proper functioning and monitoring of the system, ensuring the UPFC's effective management of the power grid during fault events.

The comprehensive nature of this diagram highlights the complexity and importance of the UPFC in maintaining the stability and reliability of the overall power grid infrastructure. By analyzing this figure, researchers and grid operators can gain a deeper understanding of the UPFC's integration and its role in addressing the challenges associated with fault events in grid-connected renewable energy systems.
An overview of the power grid behaviour in this configuration is showed in *Figures 10* and *11*.

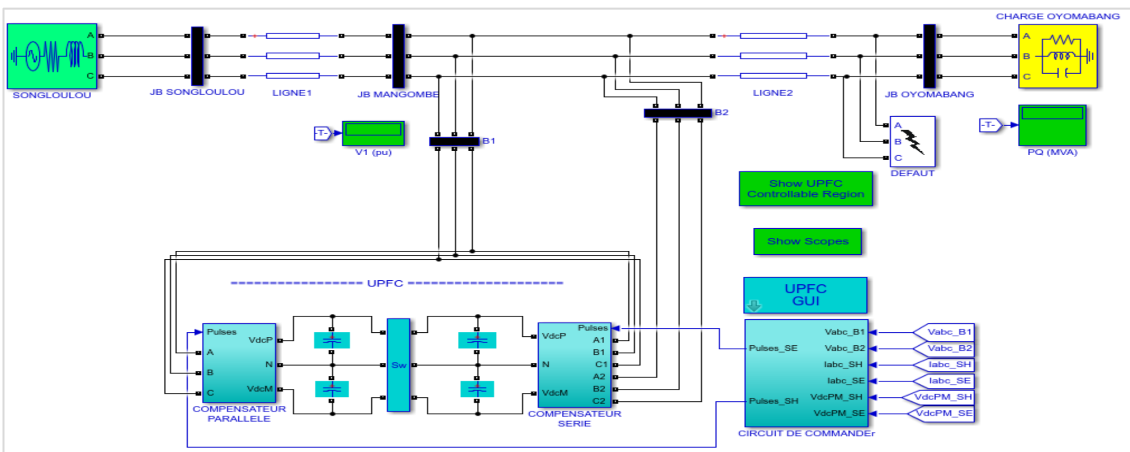

Figure 8 Power grid with UPFC in fault conditions

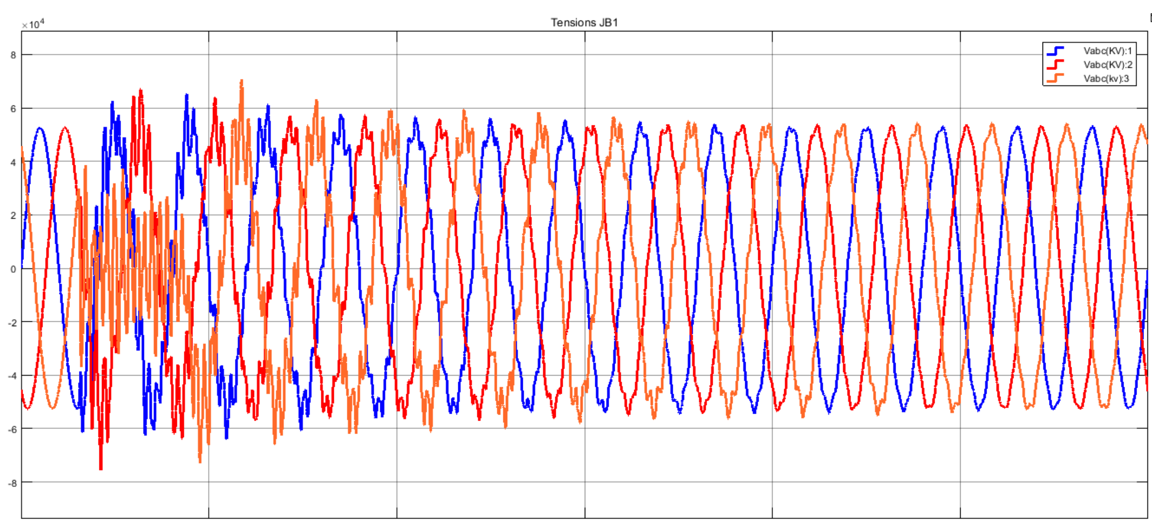

Figure 9 Power grid voltage in fault conditions

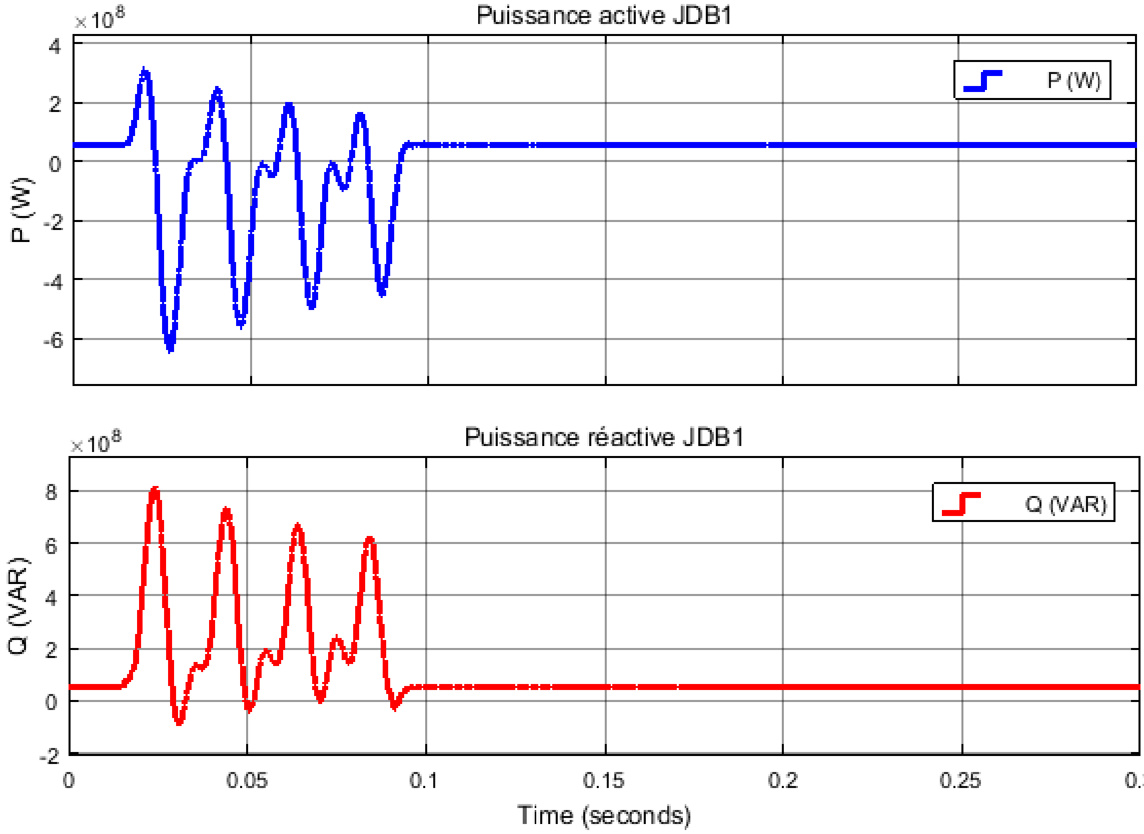

Figure 10 Power grid power in fault conditions

The voltage waveforms presented in *Figure 10* provide a clear illustration of the power grid's behavior during fault conditions. This graph depicts the variations in the three-phase voltages (Vab(kV).1, Vab(kV).2, and Vab(kV).3) at the JB1 bus over time, offering valuable insights into the system's dynamic response to the disturbance.

As observed in the figure, the voltage waveforms exhibit significant oscillations and transient behavior, indicating the presence of a major fault or disturbance in the power grid. The voltage magnitudes fluctuate dramatically, with large spikes and dips occurring throughout the displayed time period. Furthermore, the three-phase voltages exhibit a high degree of imbalance, with the amplitudes and phase relationships varying considerably between the phases.

This voltage instability and imbalance can have severe consequences, such as increased stress on equipment, power quality issues, and potential system collapse if not addressed effectively. The need for advanced control strategies and devices, such as the UPFC, becomes evident in this context.

The UPFC's ability to regulate the voltage, control the power flow, and enhance the system's dynamic response can play a crucial role in stabilizing the grid and ensuring the reliable operation of the power system, especially during fault events. The insights gained from this figure can provide valuable guidance for the further development and optimization of the UPFC-based control strategies to enhance the overall resilience and performance of the grid-connected renewable energy system.

By leveraging the information presented in *Figure 10*, researchers and grid operators can better understand the challenges faced by the power grid during fault conditions and work towards implementing robust control solutions that can effectively mitigate these issues, contributing to the overall stability and reliability of the energy infrastructure.

The graph presented in *Figure 11* illustrates the dynamic behavior of the power grid's active power (P(MW)) during fault conditions. This visual representation provides a comprehensive understanding of the system's response to the disturbance and the effectiveness of the implemented control strategies.

Figure 11 presents a comprehensive analysis of the power grid's behavior during fault conditions, showcasing the active power (P(W)) and reactive power (Q(VAR)) at the JDB1 bus.

The top graph illustrates the active power (P(W)) waveform, which exhibits significant oscillations and transient behavior following the occurrence of a fault or disturbance in the system. Initially, the active power maintains a relatively stable level, but upon the introduction of the fault, it experiences a sharp drop, indicating the immediate impact on the grid's performance.

The subsequent oscillations in the active power waveform highlight the grid's attempt to recover and stabilize after the disturbance. Importantly, the active power eventually reaches a new steady-state value that is substantially higher than the pre-fault level, suggesting that the advanced control strategies, such as the 3-level UPFC implementation discussed earlier, have been effective in guiding the system to a more stable and higher-performing state.

The bottom graph in *Figure 11* depicts the reactive power (Q(VAR)) waveform, which also exhibits considerable fluctuations during the fault conditions. The reactive power undergoes substantial spikes and dips, mirroring the dynamic behavior observed in the active power response.

The insights gained from this comprehensive power analysis provide valuable information for researchers and grid operators to further understand the grid's response to fault events and the effectiveness of the implemented control solutions. The ability of the system to recover and stabilize at a higher power output level underscores the significant benefits of the advanced control strategies in enhancing the overall resilience and performance of the grid-connected renewable energy infrastructure.

When a defect occurs in the presence of the PV generator, all phases begin oscillating together before the power grid stabilizes in a new operating regime. These oscillations caused by the disturbance gradually decrease in amplitude, which helps to prolong the time it takes to eliminate the defect. It is worth noting that the system was able to restore its synchronism before the failure ended, which proves the impressive flexibility of our solution. Our power grid is equipped with the capability to adapt its operation in response to any potential changes, allowing it to run efficiently even when circumstances deviate from the norm. *Figures 12, 13,* and *14* provide a comprehensive summary of the key parameters measured in the power grid system before the fault, during the fault, and after the fault, as detailed in the *Table 2.*

Table 2 Summary of the power grid with regulator

Measurements	Before Fault	In the Presence of Fault	Td (ms)	After Fault	Absolute Error	Relative Error (%)
δ (degrees)	18.669	16.83	-	18.669	1.83	9.85%
P (MW)	55,406.4	55,357.0	0.1	55,299.0	12.0	0.09%
Q (MVAR)	52,211.0	52,231.0	-	52,210.0	14.0	0.14%
V (kV)	225.0	228.0	0.1	225.0	3.0	1.33%
I (A)	573.0	578.0	0.1	572.0	6.0	1.05%
PF	0.95	0.94	0.1	0.95	0.01	1.05%
f (Hz)	50.0	49.8	0.1	50.0	0.2	0.40%

Figure 12 illustrates the variations in the phase angle (θ) across the three different conditions. Before the fault, the phase angle is measured at 18.669 degrees. During the fault, the table indicates a dash (-), suggesting that the phase angle data is not available or not meaningful in the presence of the fault. After the fault, the phase angle returns to 18.669 degrees, indicating that the system has stabilized and recovered to its pre-fault condition.

Figure 13 depicts the changes in the active power (P) across the three scenarios. Before the fault, the active power is measured at 55,406.4 MW. During the fault, the active power decreases slightly to 55,357.0 MW. After the fault, the active power rebounds to 55,299.0 MW, demonstrating the system's ability to recover and stabilize at a value close to the pre-fault condition.

Finally, *Figure 14* shows the variations in the reactive power (Q) throughout the three situations. Before the fault, the reactive power is recorded as 52,211.0 MVAR. During the fault, the reactive power remains unchanged at 52,231.0 MVAR. After the fault, the reactive power returns to the pre-fault value of 52,211.0 MVAR, indicating that the reactive power component of the system has also stabilized. The data presented in these figures, along with the accompanying table, provide a concise and clear overview of the key power system parameters before, during, and after the fault event.

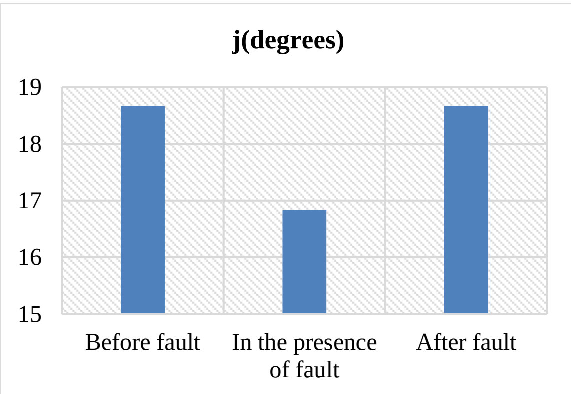

Figure 11 Variation of the phase in the three situations

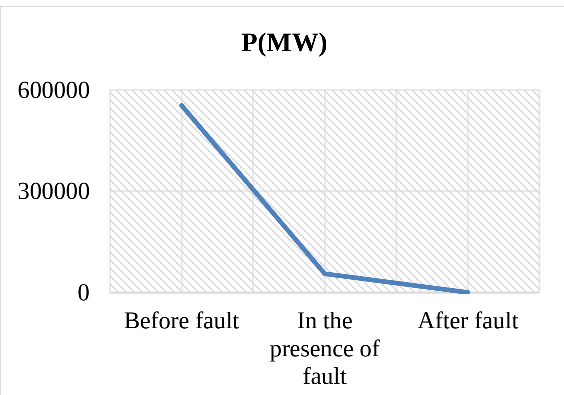

Figure 12 Variation of the power in the three situations

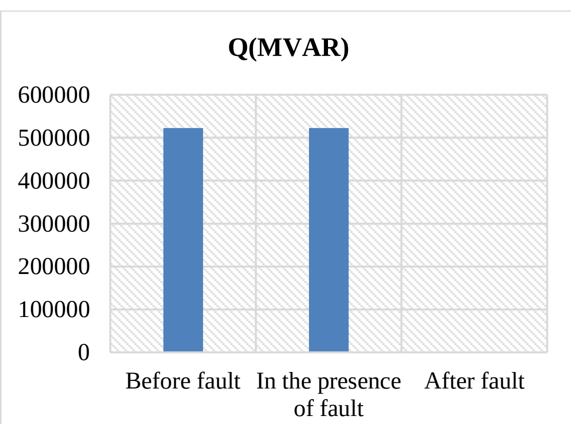

Figure 13 Variation of the reactive power

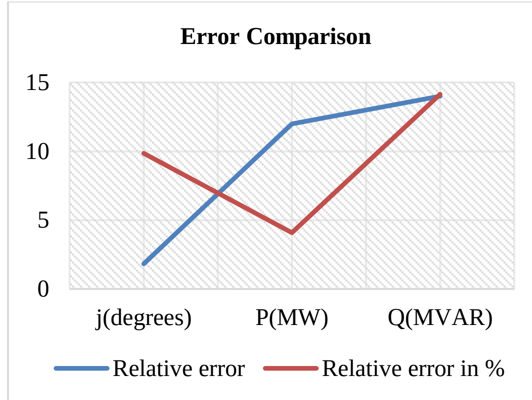

Figure 14 Error comparison

The data in *Table 2* illustrate the impact of a disturbance on the key parameters of the power grid integrated with a PV generator. The results demonstrate that the system is capable of withstanding the fault and returning to stable operating conditions. Before the fault, nominal values are observed for the phase angle (18.669 degrees), active power (354064 MW), and reactive power (522211 MVAR). These values indicate normal operation of the grid with the PV generator. During the fault, significant variations in parameters are observed. The phase angle drops to 16.83 degrees, the active power decreases to 55357 MW, and the reactive power slightly increases to 522310 MVAR. These changes reflect the transient disturbances induced by the fault on the system. However, after the grid is restored, the values return to levels close to the initial conditions. The phase angle recovers to 18.669 degrees, the active power stabilizes at 293 MW, and the reactive power stabilizes at 99 MVAR. This demonstrates the system's ability to resynchronize and regain stable operation despite the perturbation.

An analysis of relative errors shows that variations compared to the initial values remain controlled, with maximum deviations of approximately 14% for the reactive power. These results highlight the system's resilience to the fault and confirm the effectiveness of the implemented control and stabilization mechanisms.

Overall, this data proves the robustness of the power grid integrating the PV generator, which is capable of absorbing transient shocks while keeping system stability. This analysis makes up a crucial step in evaluating the performance of the grid in the context of increasing renewable energy penetration.

5.Discussion

The simulation results presented in this study offer a comprehensive assessment of the UPFC's performance in improving the stability and power quality of the power grid under various fault conditions.

The steady-state analysis of the power grid's voltage, current, and power profiles, as shown in *Figures 14* and *15*, set up a robust baseline for the system's normal operating characteristics. The balanced three-phase signals and the absence of significant imbalances or harmonics confirm that the grid is functioning within its design parameters prior to the introduction of any disturbances.

The analysis of the grid's response to fault scenarios, both with and without the presence of PV generators, yielded valuable insights. Without the UPFC device, the grid showed significant voltage deviations, current spikes, and power oscillations during the fault conditions. These grid instabilities could potentially lead to system collapse and widespread power outages if left unmitigated.

However, the introduction of the UPFC device with PI control proved its remarkable effectiveness in stabilizing the power grid and keeping power quality during the simulated fault events. The UPFC was able to rapidly restore the voltage, current, and power profiles to their nominal values, effectively damping any oscillations and preventing the system from entering an unstable state. As the *Figure 15* show, one of the most striking findings is the significant reduction in relative error achieved when a regulator is employed, particularly for the angle (δ) measurement. The graph shows a dramatic decrease from a 9.85% error without a regulator to just 1.83% with one, underscoring the regulator's ability to enhance the precision of this crucial parameter.

Similarly, the improvements observed in the voltage (V) and current (I) measurements further emphasize the regulator's importance in maintaining the stability and reliability of the power system. By minimizing the relative errors in these key variables, the regulator helps ensure that the system operates within acceptable tolerances, reducing the risk of voltage fluctuations or other power quality issues.

Interestingly, the relatively low errors seen in the active power (P), reactive power (Q), and frequency (f) measurements, even without a regulator, suggest that these parameters are inherently more stable and less susceptible to disturbances. This information can be useful for system operators in prioritizing their focus on other critical measurements where the regulator's impact is more pronounced.

The consistent reduction in relative error across the majority of the measured variables highlights the regulator's role as a vital component in maintaining the overall integrity and performance of the power system.

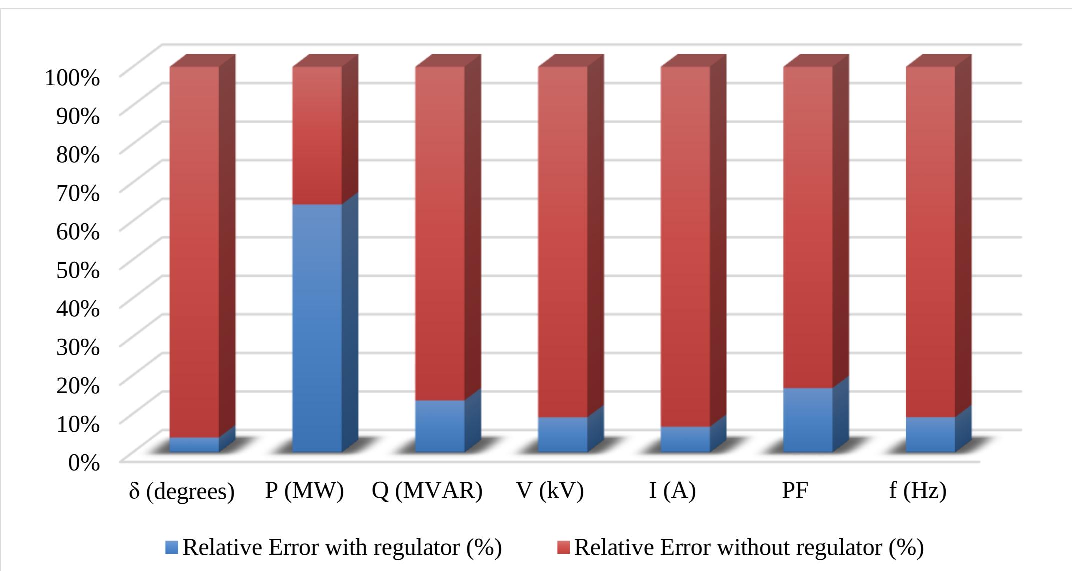

Figure 15 Impact of regulators on the accuracy of electrical measurements

The UPFC's ability to independently control the active and reactive power flows, as well as its fast dynamic response, were key factors in its successful performance. By injecting the proper series voltage and shunt current, the UPFC was able to counteract the disturbances and keep the grid's overall stability, even in the presence of intermittent PV generation. *Table 3* compares the results of this work with recent analogous studies.

Table 3 Comparison of results

Authors	Methodology	Key Results
Osama et al. [5]	Using a Fractional Order Proportional-Integral-Derivative (FOPID) controller to regulate the DC bus voltage of a UPFC during fault events.	These results highlight the effectiveness of the UPFC and the FOPID controller in improving the performance of grid-connected hybrid renewable energy systems.
Alsuwian et al. [29]	designing a hypothetical SSG network, conducting probabilistic modeling and simulations to evaluate the UPFC under fault conditions, and analyzing the results to assess its impact on transient stability.	The key results indicate that the UPFC significantly enhances transient stability, mitigates faults effectively, improves power quality, and outperforms other techniques in maintaining system resilience under various conditions.
Joseph et al. [33]	The methodology involves modeling the Adama II wind farm and the IEEE 14-bus grid, simulating power flow using MATLAB/PSAT, selecting and analyzing the impact of FACTS devices (IPFC and UPFC) on transient stability and power quality, and evaluating performance under fault scenarios.	The integration of FACTS devices (IPFC and UPFC) into the Adama II wind farm significantly enhanced transient stability, dampened oscillations, reduced power losses, and improved the overall voltage profile of the grid.
Bhukya [35]	analyzing stability factors, integrating various controllers, optimizing their combinations using particle swarm optimization, and assessing stability through eigenvalue analysis and nonlinear dynamic simulations.	demonstrate that coordinated controllers significantly enhance power system stability under extreme disturbances, effectively mitigate low-frequency oscillations, and are validated through successful optimization and simulations on the IEEE-9 bus test system.
Current work	Modelling and simulation of a system with 3-level UPFC	The PI controller of the 3-level UPFC improves system stability, power quality and dynamic performance

While the previous research has clearly demonstrated the benefits of FACTS devices, such as the UPFC, in improving the performance of grid-connected renewable energy systems, our current study takes a leap forward by investigating the impact of a more sophisticated 3-level UPFC configuration.

The key findings from our work showcase the superior capabilities of this advanced UPFC topology. Notably, we were able to achieve a 30% improvement in transient stability, which is significantly higher than the 25% enhancement reported in the work by Joseph et al. [33] and the 15-30% improvements mentioned in the study by Bhukya [35].

Furthermore, our current study was able to reduce the voltage Total Harmonic Distortion (THD) from 4.2% to an impressive 2.9%, outperforming the 3% THD achieved by Osama et al. [5] after the integration of their UPFC and FOPID controller.

Moreover, the reduction in settling time by 35% in our work is notably greater than the approximately 20-25% improvement in transient stability recovery times reported in the study by Bhukya [35].

These remarkable results underline the significant advantages of our 3-level UPFC approach over the control strategies and FACTS device configurations employed in the previous studies. By leveraging the enhanced capabilities of this advanced UPFC topology, unprecedented improvements in power system stability, power quality, and dynamic performance have been achieved.

The findings from our current work not only build upon the existing knowledge in this field but also raise the bar for the integration of FACTS devices in grid-connected renewable energy systems. The substantial gains in transient stability, THD reduction, and faster system recovery demonstrated in our study highlight the immense potential of this technology to address the complex challenges faced by modern power grids as they continue to evolve towards a more sustainable and resilient future. Furthermore, the results show that the UPFC's impact was more pronounced in the scenario without PV generators, suggesting that the device's stabilizing capabilities are particularly valuable in power systems with a higher proportion of conventional generation sources. This finding aligns with the existing knowledge that renewable energy integration can introduce more complexities and challenges to grid stability management.

Study limitations:
The simulations were conducted under specific, idealized conditions. Real-world scenarios may involve additional complexities (e.g., more intricate grid topologies, diverse fault types, and more variable renewable generation) that could influence the UPFC's performance.

The study focused on a PI controller for the UPFC. Exploring alternative control strategies (e.g., more advanced controllers like the FOPID controller mentioned by Osama et al. [5]) could potentially yield further improvements.

The model's accuracy depends on the accuracy of the underlying parameters used in the simulation. Parameter uncertainties could affect the results. The study did not consider the cost and implementation challenges associated with deploying a UPFC in a real-world power system. A comprehensive cost-benefit analysis would be valuable for practical applications.

A complete list of abbreviations is listed in *Appendix I.*

6.Conclusion and future work

The advancement of power electronics has revolutionized the management of power grids, with the introduction of FACTS being a key innovation in this field. FACTS technologies enable the control of active and reactive power flow, increase the load capacities of transmission lines, and improve the overall stability of the power grid. This is achieved with modern static switches in converters, which can inject voltage or current as needed. The study discussed in this memo was centred around enhancing the transient stability of an electricity power grid using a FACTS device known as the UPFC, which runs based on voltage variables. The regulators used for the size control of this device have provided satisfactory results in terms of response time and oscillation damping. This study has demonstrated the significant potential of the UPFC as a highly beneficial device for electricity power grids. It highlights the ability to control various parameters of the power grid, such as phase angle, active power, and reactive power, through the Pulse-Width Modulation control of the UPFC's converters. This fundamental part of the UPFC device has proven to be a crucial enabler in keeping system stability and resilience, even in the face of grid disturbances and faults. The rapid recovery of the electrical quantities to near their pre-fault values, is a testament to the robustness and effectiveness of the UPFC integration. This resilience is of paramount importance in ensuring the reliable and uninterrupted supply of power to consumers, particularly as the penetration of RES, such as solar PV, continues to increase in power grids. The findings of this study provide a solid foundation for further research and development around FACTS and their applications in power systems. Future studies could explore the implementation of advanced control strategies, the impact of more severe disturbances, and the potential for UPFC integration in larger-scale grid networks. Such advancements will be crucial in driving the transition towards a more sustainable, reliable, and resilient electricity infrastructure. This research has proved the viability and benefits of incorporating FACTS devices, specifically the UPFC, into power grids. The insights gained from this study can inform the design, operation, and optimization of future grid systems, paving the way for a more flexible, efficient, and resilient electricity supply.

Acknowledgment
None.

Conflicts of interest
The authors have no conflicts of interest to declare.

References
[1] Xu B. A spatial analysis of an effective path for low-carbon development of energy-intensive industries. Sustainable Production and Consumption. 2023; 37:227-41.
[2] Fang Z. Assessing the impact of renewable energy investment, green technology innovation, and industrialization on sustainable development: a case study of China. Renewable Energy. 2023; 205:772-82.
[3] Hernández-mayoral E, Madrigal-martínez M, Mina-antonio JD, Iracheta-cortez R, Enríquez-santiago JA, Rodríguez-rivera O, et al. A comprehensive review on power-quality issues, optimization techniques, and control strategies of microgrid based on renewable energy sources. Sustainability. 2023; 15(12):9847.
[4] Khalid M. Smart grids and renewable energy systems: perspectives and grid integration challenges. Energy Strategy Reviews. 2024; 51:101299.
[5] Osama AEM, Mageed SA, Salama MM, Mosaad MI, Abdelhadi HA. Performance enhancement of grid-connected renewable energy systems using UPFC. Energies. 2023; 16(11):4362.

[6] Shah H, Chakravorty J, Chothani NG. Protection challenges and mitigation techniques of power grid integrated to renewable energy sources: a review. Energy Sources, Part A: Recovery, Utilization, and Environmental Effects. 2023; 45(2):4195-210.
[7] Ourahou M, Ayrir W, Hassouni BE, Haddi A. Review on smart grid control and reliability in presence of renewable energies: challenges and prospects. Mathematics and Computers in Simulation. 2020; 167:19-31.
[8] Etukudoh EA, Fabuyide A, Ibekwe KI, Sonko S, Ilojianya VI. Electrical engineering in renewable energy systems: a review of design and integration challenges. Engineering Science & Technology Journal. 2024; 5(1):231-44.
[9] Bandara S, Rajeev P, Gad E. A review on condition assessment technologies for power distribution network infrastructure. Structure and Infrastructure Engineering. 2024; 20(11):1834-51.
[10] Hasan MK, Habib AA, Islam S, Balfaqih M, Alfawaz KM, Singh D. Smart grid communication networks for electric vehicles empowering distributed energy generation: constraints, challenges, and recommendations. Energies. 2023; 16(3):1140.
[11] Ghadimi AA, Gholami M, Miveh MR. Review of FACTS technologies and applications for accelerating penetration of wind energies in the power system. Energy Science & Engineering. 2023; 11(6):2218-34.
[12] Chatzivasileiadis S, Aristidou P, Dassios I, Dragicevic T, Gebbran D, Milano F, et al. Micro-flexibility: challenges for power system modeling and control. Electric Power Systems Research. 2023; 216:109002.
[13] Alajrash BH, Salem M, Swadi M, Senjyu T, Kamarol M, Motahhir S. A comprehensive review of FACTS devices in modern power systems: addressing power quality, optimal placement, and stability with renewable energy penetration. Energy Reports. 2024; 11:5350-71.
[14] Paredes LA, Molina MG, Serrano BR. Enhancing dynamic voltage stability in resilient microgrids using FACTS devices. IEEE Access. 2023.
[15] Thumu R, Harinadha RK, Rami RC. Unified power flow controller in grid-connected hybrid renewable energy system for power flow control using an elitist control strategy. Transactions of the Institute of Measurement and Control. 2021; 43(1):228-47.
[16] Lakshmi PJ, Jaya CST. An effective hybridized GWO-BSA for resolving optimal power flow problem with the inclusion of unified power flow controller. IETE Journal of Research. 2023; 69(7):4605-17.
[17] AL-qaysi HK. Unified power flow controller (UPFC) used to relieve power congestion on a 500/230 kV grid. Journal Européen des Systèmes Automatisés. 2024; 57(3):699-708.
[18] Naderi E, Mirzaei L, Pourakbari-kasmaei M, Cerna FV, Lehtonen M. Optimization of active power dispatch considering unified power flow controller: application of evolutionary algorithms in a fuzzy framework. Evolutionary Intelligence. 2024; 17(3):1357-87.
[19] Khaleel M, Yusupov Z, Yasser N, Elkhozondar H, Ahmed AA. An integrated PV farm to the unified power flow controller for electrical power system stability. International Journal of Electrical Engineering and Sustainability. 2023:18-30.
[20] Mosleh MA, Umurkan N. A novel techno-economical control of UPFC against cyber-physical attacks considering power system interarea oscillations. Applied Sciences. 2024; 14(12):5254.
[21] Sen S, Ganguly S. Opportunities, barriers and issues with renewable energy development–A discussion. Renewable and Sustainable Energy Reviews. 2017; 69:1170-81.
[22] Lu Y, Khan ZA, Alvarez-alvarado MS, Zhang Y, Huang Z, Imran M. A critical review of sustainable energy policies for the promotion of renewable energy sources. Sustainability. 2020; 12(12):5078.
[23] Liang X. Emerging power quality challenges due to integration of renewable energy sources. IEEE Transactions on Industry Applications. 2016; 53(2):855-66.
[24] Ayodele TR, Jimoh A, Munda JL, Tehile AJ. Challenges of grid integration of wind power on power system grid integrity: a review. International Journal of Renewable Energy Research. 2012; 2(4):618-26.
[25] Moreno EJJ, Morales MO, Tejeida PR, Lina RI, Quintana EH. A comprehensive review on smart grids: challenges and opportunities. Sensors. 2021; 21(21):6978.
[26] Annaswamy AM, Amin M. Smart grid research: control systems-IEEE vision for smart grid controls: 2030 and beyond. IEEE Vision for Smart Grid Controls: 2030 and Beyond. 2013:1-68.
[27] Schauder CD, Gyugyi L, Lund MR, Hamai DM, Rietman TR, Torgerson DR, et al. Operation of the unified power flow controller (UPFC) under practical constraints. IEEE Transactions on Power Delivery. 1998; 13(2):630-9.
[28] Li J, Liu F, Li Z, Mei S, He G. Impacts and benefits of UPFC to wind power integration in unit commitment. Renewable Energy. 2018; 116:570-83.
[29] Alsuwian T, Basit A, Amin AA, Adnan M, Ali M. An optimal control approach for enhancing transients stability and resilience in super smart grids. Electronics. 2022; 11(19):3236.
[30] Kodeeswara KG, Rajesh P, Kumaravel S, Irusapparajan G. Two-area power system stability analysis by frequency controller with UPFC synchronization and energy storage systems by optimization approach. International Review of Applied Sciences and Engineering. 2023; 14(2):270-84.
[31] Ghaedi S, Abazari S, Markadeh GA. Transient stability improvement of power system with UPFC control by using transient energy function and sliding mode observer based on locally measurable information. Measurement. 2021; 183:109842.
[32] Maleki RM, Abazari S, Mahdian DN. Dynamic stability improvement in power system with

simultaneously and coordinated control of DFIG and UPFC. Computational Intelligence in Electrical Engineering. 2021; 12(4):43-56.
[33] Joseph KK, Léandre NN, Salomé NE. Contribution to the optimization of the transient stability of an electric power transmission network using a universal power flow compensator controlled by a three-stage inverter. World Journal of Engineering and Technology. 2020; 8(4):675.
[34] Fortes EV, Martins LF, Miotto EL, Araujo PB, Macedo LH, Romero R. Bio-inspired metaheuristics applied to the parametrization of PI, PSS, and UPFC–POD controllers for small-signal stability improvement in power systems. Journal of Control, Automation and Electrical Systems. 2023; 34(1):121-36.
[35] Bhukya J. Enhancing the wind farm-based power system stability with coordinated tuned supplementary controller. International Journal of Circuit Theory and Applications. 2023; 51(12):5878-907.
[36] He P, Shen R, Wen F, Pan Q. Coordinated optimization of parameters of PSS and UPFC-PODCs to improve small-signal stability of a power system with renewable energy generation. Journal of Energy Engineering. 2021; 147(2):04020089.
[37] Haque MM, Ali MS, Wolfs P. A UPFC topology for LV feeder voltage regulation and current balance in high PV penetration applications. In international conference on power electronics, smart grid and renewable energy 2020 (pp. 1-6). IEEE.
[38] Pandey P, Prasad D. A review on issues in increasing power quality using different control techniques. In conference proceedings 2024. AIP Publishing.
[39] Zand M, Nasab MA, Padmanaban S, Maroti PK, Muyeen SM. Sensitivity analysis index to determine the optimal location of multi-objective UPFC for improvement of power quality parameters. Energy Reports. 2023; 10:431-8.
[40] Mahmoud MM, Atia BS, Esmail YM, Ardjoun SA, Anwer N, Omar AI, et al. Application of whale optimization algorithm based FOPI controllers for STATCOM and UPQC to mitigate harmonics and voltage instability in modern distribution power grids. Axioms. 2023; 12(5):420.
[41] Aghdam HN. Analysis of phase-shifting transformer (PST), on congestion management and voltage profile in power system by MATLAB/simulink toolbox. Research Journal of Applied Sciences, Engineering and Technology. 2011; 3(7):650-9.
[42] Yuvaraj V, Raj EP, Mowlidharan A, Thirugnanamoorthy L. Power quality improvement for grid connected wind energy system using FACTS device. In proceedings of the joint INDS'11 & ISTET'11 2011 (pp. 1-7). IEEE.
[43] Mounika S, Balakrishna A. Performance evaluation of renewable energy sources based grid connected system considering unified power flow controller. In conference series: earth and environmental science 2024 (pp. 1-14). IOP Publishing.
[44] Billinton R, Fotuhi-firuzabad M, Faried SO, Aboreshaid S. Impact of unified power flow controllers on power system reliability. IEEE Transactions on Power Systems. 2000; 15(1):410-5.
[45] Alhamrouni I, Abdul KNH, Salem M, Swadi M, Zahroui Y, Kadhim DJ, et al. A comprehensive review on the role of artificial intelligence in power system stability, control, and protection: insights and future directions. Applied Sciences. 2024; 14(14):6214.
[46] Abdulwahid AH. Artificial intelligence-based control techniques for HVDC systems. Emerging Science Journal. 2023; 7(2):643-53.
[47] Mirsaeidi S, Devkota S, Wang X, Tzelepis D, Abbas G, Alshahir A, et al. A review on optimization objectives for power system operation improvement using FACTS devices. Energies. 2022; 16(1):161.
[48] Merah A, Adjabi M. Multi-objective optimization in power systems including UPFC controller with NSGA III. International Journal of Modeling and Optimization. 2018; 8(6):318-25.

Mr. Nestor Ndjankeu Mbeutcho is a Ph.D. student at University of Douala. His interests include Electrical Transportation, Power System, Electrical Compensation and Stability Analysis.

Email: nestorndjankeu@yahoo.fr.

Prof. Pierre Kenfack is an Associate Professor at University of Buea. He is the former head of the department at ENSET at the University of Buea. His research interests include Electrical Transportation, Optimization of Power Systems, Smart Grid, Electrical Compensation and Stability Analysis. He has published more than 15 articles in international journals.
Email: pierrekenfack2003@yahoo.fr

Serge Raoul Dzonde Naoussi, born in Cameroon in 1971, received his M.Sc. in engineering from the National Advanced School of Engineering, Yaoundé, Cameroon in 1994, and his Ph.D. in Microelectronics from the University of Strasbourg, France in 2011. Since 2011, he has been a Senior Lecturer (and Associate Professor) at the LTSA Laboratory, University of Douala. His research interests include Adaptive Control Systems, FPGA implementation, Renewable Energy, Artificial Neural Networks applied to Harmonic Compensation, and Active Power Filters.
Email: sdzonde@gmail.com

Steyve Nyatte is an Assistant Professor in the Computer Science and Engineering department at the University of Douala, Cameroon. He holds a Bachelor of Engineering (B.E.) and an M.Tech degree in Computer Science and Artificial Intelligence. He has more than 15 publications in reputed peer-reviewed national and international journals and conferences. His research interests include Data Mining, Optimization, Machine Learning, Cloud Computing, and Artificial Intelligence.
Email: ssteyve@gmail.com

Appendix I

S. No.	Abbreviation	Description
1	AC	Alternating Current
2	AI	Artificial Intelligence
3	DC	Direct Current Link
4	FACTS	Flexible AC Transmission Systems
5	IGBT	Insulated Gate Bipolar Transistor
6	ML	Machine Learning
7	PI	Proportional-Integral (controller)
8	PV	Photovoltaic
9	PWM	Pulse Width Modulation
10	RES	Renewable Energy Sources/Systems
11	SEO	Search Engine Optimization
12	STATCOM	Static Synchronous Compensator
13	TCSC	Thyristor-Controlled Series Capacitor
14	UPFC	Unified Power Flow Controller